Optimized Design of Multilayer Barrier Films Incorporating a Reactive Layer. I. Methodology of Ingress Analysis

Stanislav E. Solovyov, Anatoliy Y. Goldman

Department of Materials and Processing, Alcoa Closure Systems International, Incorporated, 1205 Elmore Street, Crawfordsville, Indiana 47933

Received 25 October 2004; accepted 30 August 2005
DOI 10.1002/app.23433
Published online 3 February 2006 in Wiley InterScience (www.interscience.wiley.com).

ABSTRACT: A new method for the analysis of oxygen ingress into packages and optimized design solutions for multilayer barrier films incorporating an immobile noncatalytic oxygen scavenger within one of the layers are presented in this three-part series. The results are based on the theoretical framework of transient permeation through a dense reactive medium with a finite solute scavenging capacity. The target application was flexible and rigid plastic packaging for oxygen-sensitive products, and the goal was the minimization of oxygen ingress into the package within a predetermined timeframe. A predictive model for oxygen ingress was developed, and practical recommendations for the selection of layer material properties, layer sequencing, and placement of the scavenger within a layer to achieve this goal are provided. Part I introduces the concepts of reference and steady-state lag times for passive barriers to gas permeation. These concepts are expanded to include the scavenger exhaustion lag time for noncatalytic reactive barriers with an instantaneous scavenging reaction. The steady-state lag time concept is applied to the characterization of noncatalytic reactive barrier solutions with finite rates of the scavenging reaction using transient effective flux dynamics and the model of solute ingress into the package. The model is based on the semipermeable reaction wavefront concept, which we developed. The corresponding passive-to-reactive film transition and its effect on the lag times are discussed. © 2006 Wiley Periodicals, Inc. J Appl Polym Sci 100: 1940–1951, 2006

Key words: barrier; membranes; transitions

INTRODUCTION

Despite the numerous documented advantages of thermoplastic polymers over conventional packaging materials, such as metals, glass, and paper, the polymers used for flexible and rigid contained environment packaging have some serious deficiencies that are apparent in commercial applications. Among the most significant of these disadvantages is the insufficient barrier provided by most thermoplastic materials to the permeation of atmospheric gases, ethylene, and water vapor. Although metal and glass containers provide nearly an absolute barrier to diffusive mass transport between the environments separated by a container wall, plastic packaging materials have permeation rates that are orders of magnitude higher for most gases. In particular, high rates of oxygen ingress lead to a reduced shelf life for packaged products and higher costs to food processors and retail customers. Active packaging is a relatively new development field that among other goals, aims to overcome the permeability limitations of plastic materials. A significant development direction in active packaging involves the incorporation of oxygen scavenging systems into packaging materials. The scavengers provide a reactive barrier to oxygen permeation to complement the passive barrier properties of the matrix polymeric material, and they can also reduce oxygen concentrations present in the package headspace. This study focused only on the unidirectional solute ingress into the package; the dynamics of headspace oxygen scavenging or bidirectional solute flux into the reactive membrane from both the environment and the package are subjects for another study.

Multilayer gas barrier films incorporating oxygen scavengers have been actively researched in the field of active packaging for food, beverage, pharmaceutical, and microelectronic applications. Numerous patents[1] have been granted that describe the particular designs of multilayer structures incorporating a scavenging layer with the goal of reducing oxygen ingress into the package. Despite many claims, however, there is a lack of theoretical understanding of what constitutes the optimal design of a multilayer barrier structure where one layer contains a reactive species able to irreversibly bind permeating oxygen. Because of the

Correspondence to: S. E. Solovyov, Multisorb Technologies, Incorporated, 325 Harlem Road, Buffalo, NY 14224 (ssolovyov@multisorb.com).

chemical nature of the solute of interest (oxygen and potentially other permanent gases), the reactions consuming it are inherently noncatalytic, that is, they always involve the simultaneous consumption or deactivation of the reactive substrate (the scavenger). Such reactions are fundamentally different from catalytic reactions (CRs) that for example, may be used for scavenging ethylene gas through catalytic polymerization or oxidation when an oxidizing agent is always present in excess. The critical difference is the finite time of barrier improvement that results from the use of noncatalytic reactions (NCRs) because of the finite reactive capacity of noncatalytic scavengers. Hence, the unstated goals of barrier film design implied by oxygen ingress reduction can be separated into extending the lifetime of the noncatalytic scavenger and reducing the effective oxygen transmission rates during that time. Although these are often conflicting targets, formulating the goal of reactive barrier designs as the achievement of minimal possible oxygen ingress during a fixed timeframe (which is application specific and may include the infinite time) allows one to develop practical solutions. This article provides practical recommendations for the selection of layer material properties, layer sequencing, and the placement of the scavenger within a layer to achieve desired targets of the lowest transient transmission rate and the longest useful life of the scavenger. The results are based on the theoretical framework we developed for transient permeation through dense reactive–passive (RP) structures.[2–4] The assumption of dense materials, as opposed to stagnant gas films and highly porous structures, is invoked to guarantee the absence of convective solute flow through the barrier; hence, only diffusive mass transport is considered.

We focused on the case of an irreversible homogeneous chemical reaction of permeating oxygen with an immobile oxygen scavenger dispersed in a polymer matrix (as a well-dispersed solid particulate system, a polymer blend, or functional reactive groups attached to the matrix polymer backbone). The analytically derived optimal design solutions use the synergetic effects of permeant diffusivity and solubility in the film material, layer sequencing, scavenger reactivity, and reactive capacity combined with the effects of the environmental conditions inside and outside the package on the effective transmission rates (TR_{eff}'s) in the reactive films and oxygen ingress during the scavenger exhaustion times.

GOVERNING EQUATIONS

What follows are the governing one-dimensional equations describing the reactive–diffusive mass transport of a solute (where C is the concentration of solute A dissolved in the polymer matrix **M**) across an essentially planar polymer membrane of uniform thickness (L) loaded with a well-dispersed immobile solute scavenger (where R is the concentration of activated reactive sites) consuming the solute in the course of the irreversible isothermal bimolecular homogeneous chemical reaction of the second order in the presence of a solute concentration difference on opposite film surfaces:

$$\frac{\partial C}{\partial t} = \frac{\partial}{\partial x}\left(D\,\frac{\partial C}{\partial x}\right) - \mu KRC \tag{1}$$

$$\frac{\partial R}{\partial t} = -KRC \tag{2}$$

where D ($\equiv D_{AM}$) is the diffusivity of solute A in the polymer matrix **M** (which is assumed to be independent of the solute concentration but potentially a discontinuous function across L if a heterogeneous multilayer structure is considered), K [$= K(T)$] is the reaction rate constant established upon instantaneous scavenger activation at time $t = 0$, and μ ($= C/R$) is the initial reactive capacity of the fully activated scavenger and is defined as the stoichiometric coefficient for the amount of the permeating species consumed by the unit amount of the scavenger [mol/mol or m^3 (STP)/mol]. Commercially available scavenging systems can be activated through different mechanisms, for example, by heat and moisture diffusion for systems based on reduced iron or by UV radiation for systems based on the oxidation of functionalized polymers in the presence of transition metal catalysts and photoinitiators. For our purposes, we do not consider scavenger activation kinetics and always assume instantaneous activation throughout the membrane thickness by some external source. Because of the focus of active packaging solutions on scavenging atmospheric oxygen, we use the terms *solute, permeant,* and *oxygen* interchangeably. The scope of our work is not limited to oxygen scavenging, however, because the same methodology can be applied to the general analysis of reactive–diffusive mass transport in polymeric films and other permeable reactive barriers.

Fixed partial solute pressures inside the package (p_{in}) and outside the package ($p_{out} > p_{in}$) outside the film were assumed to approximate common conditions in food packaging, where a physical barrier separates two unlimited environments in thermal equilibrium with a gradient of chemical potential of permeating species across the barrier. Then, with the assumption of linear sorption isotherms (Henry's law) for all polymeric materials (a generally valid assumption for permanent gases at ambient atmospheric pressures and ambient temperatures above the glass-transition temperature of polymers commonly used in commercial packaging), the equilibrium concentrations (C_{in} C_{out}) of the permeant within the inner and the outer film boundaries, respectively, were found by

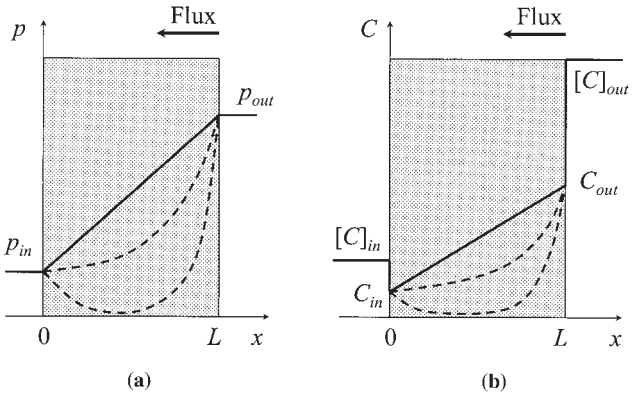

Figure 1 Typical (a) steady-state solute partial pressure and (b) concentration profiles across (—) passive and (- - -) CR membranes.

Inner film boundary (downstream):

$$x = 0,\ C(0, t) \equiv C_{\text{in}} = Sp_{\text{in}} \tag{3}$$

Outer film boundary (upstream):

$$x = L,\ C(L, t) \equiv C_{\text{out}} = Sp_{\text{out}} > C_{\text{in}} \tag{4}$$

where S is the solubility coefficient for the solute in a polymer matrix, as shown in Figure 1. The partition coefficient (H) between two adjacent solute carrier media (here, the film material and vacuum) is also often used. H is defined as the ratio of equilibrium solute concentrations in the film material and the adjacent gas phase at a specific pressure and temperature:

$$H \equiv H_{PG}(p, T) \equiv \frac{C}{[\text{C}]} \tag{5}$$

where C is the equilibrium concentration of solute A in the polymer matrix (P), and [C] is its equilibrium concentration in the adjacent gas phase (G). If H is independent of the solute pressure in the pressure range of interest, it can be calculated the same way at both the inner and outer film–gas interfaces:

$$H = \frac{C_{\text{in}}}{[\text{C}]_{\text{in}}} = \frac{C_{\text{out}}}{[\text{C}]_{\text{out}}} \tag{6}$$

Figure 1(b) shows the steady-state solute concentration profiles in the homogeneous passive and CR layers for the sample case of $H = 0.5$.

Although the dual-mode sorption model[5] is not applicable to the problem as stated because it requires modification of the diffusive part of eq. (1) and the introduction of two diffusion coefficients, one can use common nonlinear sorption isotherms such as Langmuir, Flory–Huggins, and and various forms of Braunaur–Emmet–Taylor (BET) isotherms in eqs. (3) and (4) without compromising generality of the results. This is due to the fact that we base all of the derivations on the boundary concentrations C_{in} and C_{out} within the film that instantly adjust to their adjacent environments (i.e., the solute equilibrium across the material–environment interface is assumed to always be present and instantaneous or at least very quickly established compared to the rate of reactive–diffusive processes taking place in the film). Corresponding sorption isotherm expressions can then be substituted into eqs. (3) and (4) to obtain C_{in} and C_{out}.

The chosen initial conditions correspond to the steady-state solute flux established across the initially passive membrane:

$$C(x, 0) = C_{SSP}(x) \tag{7}$$

$$R(x, 0) = R_0 \tag{8}$$

at the moment of the full scavenger activation, defined at $t = 0$ as

$$K(t) = K_A h(t) \tag{9}$$

where R_0 is the initial concentration of the scavenger in the film material, $h(t)$ is the Heaviside step function, K_A [$= K_A(T)$] is the reaction rate constant of the fully activated scavenger, and $C_{SSP}(x)$ is the steady-state solute concentration profile established within the initially passive film (with the inactivated scavenger) by $t = 0$, as shown in Figure 1(b) by a solid line. The reaction rate constants of scavenging reactions in polymer matrices are rarely directly available because they are problematic to determine in diffusion-controlled reactive systems because of measurement problems associated with falsified kinetics. One experimental method of determining the effective K in barrier films with a diffusion-controlled scavenging reaction by transient permeability measurements can be found in ref. 6.

Our conclusions are based on the matching of an analytical steady-state solution for reaction and diffusion with a stoichiometric excess of the scavenger in the multilayer film and a transient solution for the solute mass balance on the (slowly) propagating reaction wavefront consuming the scavenger and the allowance of partial permeation of the solute through it. In a partially permeable reaction wavefront, the solute is not entirely consumed by the reaction; rather, the flux of the solute in excess of the stoichiometrically reacted amount is matched on both sides of the front to eliminate solute accumulation or depletion in it. As a result, the step function approximation of the scavenger concentration representing the wavefront is ef-

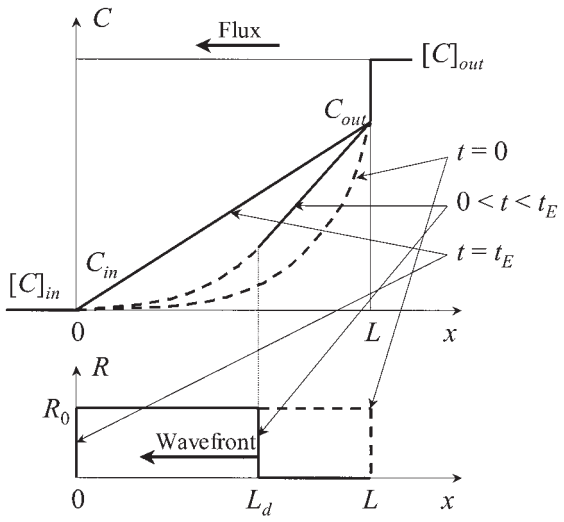

Figure 2 Dynamics of *C* and *R* values in the NCR monolayer as approximated by the SG model.

fectively widened to include the entire unreacted part of the film. This approach, hereafter called the Solovyov–Goldman (SG) model of transient permeation, is illustrated in Figure 2. A narrow reaction wavefront is present when the reaction is fast, that is, when the initial Thiele modulus [ϕ_0; also known as the Hatta number (*Ha*) or the square root of the second Damköhler number (Da^{II})] is described by

$$\phi_0 = L\sqrt{\frac{k_0}{D}} \gg 1 \tag{10}$$

where

$$k_0 = \mu K R_0 \tag{11}$$

where k_0 is the apparent pseudo-first-order finite reaction rate constant assumed for the initial concentration of the noncatalytic scavenger or for the CR not consuming the scavenger. ϕ_0 refers to the activated scavenger at 100% reactive capacity uniformly dispersed within the layer of thickness *L*. The characteristic size of the scavenger species or the reactive functional groups is assumed to be much smaller than the layer thickness for the earlier assumption of the homogeneous chemical reaction kinetics as postulated in eqs. (1) and (2) to be valid. In case of a narrow propagating reaction wavefront, the thickness of the reactive layer and the corresponding transient Thiele modulus value [$\phi(t)$] will be reduced with time until it reaches zero at the moment of complete depletion of the scavenger reactive capacity. A narrow reaction wavefront exists provided $\phi_0 > 100$, as approximately found in ref. 7 with the impermeable wavefront model; however, the solution matching technique developed in the SG model allows one to obtain meaningful approximate solutions for the transient transmission rate for much smaller ϕ_0 (>2) values with weaker diffusion control of the overall reaction rate when no well-defined reaction wavefront is present. Cases where $\phi_0 < 2$, corresponding to activation-controlled reactions, do not warrant a detailed analysis because it is easy to show[4] that the transient barrier improvement for the reactive layer with a slow scavenging reaction is negligible for practical applications on a timescale comparable to the expected product shelf life. Moreover, the steady-state lag time (as a critical barrier improvement property) has been shown to approach zero linearly with ϕ_0 as ϕ_0 drops below 1.5 when ϕ_0 is reduced by the reduction of the reactive film *L* (rather than *K*). This scenario results in the waste of all scavenger reactive capacity on the accelerated sorption and consumption of environmental oxygen with no effect on oxygen ingress into the package. These solutions, details of derivation, and the solution matching technique were described in our previous work.[2–4] We use the important results of these works without repeating the model arguments.

Figure 3 summarizes the solute ingress patterns as a function of time for homogeneous passive and reactive layers with the finite and infinite scavenging reactive capacities corresponding to noncatalytic and catalytic scavenging reactions, respectively. *Solute ingress* is defined as the amount of solute exited from the unit area of the downstream membrane boundary into the package during a specified time interval; that is, it is a cumulative measure of film barrier performance. The dashed lines in Figure 3 correspond to the steady-state initial conditions [eq. (7)], whereas solid lines correspond to the reference initial conditions when the membrane is initially solute free and the solute is suddenly introduced at the upstream boundary of the membrane at $t = 0$. The ingress dynamics through the passive film corresponding to the reaction rate constant $K = 0$ are marked with P, whereas R is used for

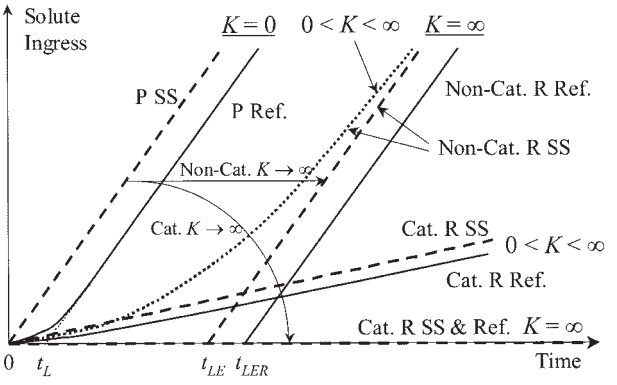

Figure 3 Dynamics of solute ingress into the package across passive (P) and reactive (R) monolayers (SS = steady state conditions; Ref. = reference conditions).

the reactive film with $K > 0$. The principal difference between the catalytic and noncatalytic scavenging reactions is shown by the arrows representing the hypothetical K increase from zero to infinity. The increase in K, constant throughout membrane thickness, is depicted because for the NCR consuming the scavenger, the apparent reaction rate $k(x,t) = \mu KR(x,t)$ is reduced with the scavenger consumption [i.e., with the transient $R(x,t)$ reduction from R_0 to 0]. The CR does not consume the scavenger; hence, k is constant during its course. The instantaneous CR ($K = \infty$) results in an everlasting absolute barrier to solute permeation, represented by zero ingress. In this case, the steady-state and reference initial conditions result in the same behavior because the zero flux condition is established instantly when the reaction is triggered at $t = 0$. When $0 < K < \infty$, the rate of ingress is generally nonzero (depending on ϕ_0 and the boundary conditions), and there is a delay in the establishment of the steady-state permeation for the reference initial conditions. This delay is caused by the finite rate of solute diffusion in dense membranes in the absence of a convective solute flow. The steady state is represented by a linear dependence of the solute ingress on time as $t \to \infty$. For the passive membrane ($K = 0$), this delay is called the *reference lag time* (t_L), as shown in Figure 3. Obviously, there is no lag time for the passive membrane in the steady-state initial conditions, that is, $t_L^{SS} = 0$.

The NCR with an infinitely large apparent initial reaction rate [$k_0 = \infty$ ($\phi_0 = \infty$)] provides the absolute barrier to solute permeation but only for a limited time. After that time, the lag time due to noncatalytic scavenging reaction at the steady-state initial conditions (t_{LR}^{SS}), the reactive capacity of the scavenger is reduced to zero, and the material reverts to a passive permeation pattern with the same ingress rate as before $t = 0$. To guarantee that it is assumed that the solute scavenging reaction does not significantly affect the solute transport properties of the matrix polymer containing the scavenger. The reference NCR lag time t_{LR}^{ref} is longer than t_{LR}^{SS} and equal to the sum of t_{LR}^{SS} and t_L, as demonstrated in ref. 8. We are primarily interested in the case of NCR with a finite rate constant of $0 < K < \infty$: its breakthrough curve for the steady-state initial conditions is shown in Figure 3 as a dotted line. The steady-state permeation in this case is only asymptotically achieved at infinite times; hence, we had to consider unsteady permeation dynamics or transient permeation within any finite timeframe of interest. This case is fundamentally different from that of the CR with a finite rate that results in the quick establishment of the steady state and that has been widely studied in the literature (e.g., ref. 9). The implications of this difference for the optimal design of multilayer reactive films of practical importance form the subject of this work.

NORMALIZATION OF THE PARAMETERS

We introduced scaling parameters corresponding to $\phi_0 = 1$ in the reactive layer and a solute partial pressure difference of 0.2 atm, representing oxygen in ambient air outside and no free oxygen inside the package (maintained):

$$\text{Partial pressure of oxygen inside the package:} \quad p_{in} = 0 \text{ Pa}$$

$$\text{Partial pressure of oxygen in ambient air:} \quad p_{out} = 0.2 \times 10^5 \text{ Pa}$$

Film layer thickness:
$L = 10^{-4}$ m
Oxygen diffusivity in the polymer:
$D = 10^{-12}$ m^2 s^{-1}
Oxygen solubility coefficient:
$S = 10^{-6}$ m^3 (STP) m^{-3} Pa^{-1}
Apparent initial reaction rate:
$k_0 = \mu K R_0 = 10^{-4}$ s^{-1}
Scavenging capacity of film material:
$\mu R_0 = 1$ m^3 (STP) m^3
Oxygen flux (negative flux scaling):
$J = -10^{-10}$ m^3 (STP) m^{-2} s^{-1} (12)

All values reported hereafter are normalized to values in eq. (12) to facilitate comparison between the kinetic and thermodynamic properties of the polymer film matrix and the solute scavenging chemistries. Note the negative flux scaling (to report positive flux values) and the normalized steady-state value of the atmospheric oxygen flux ($J^P = 2$) through the reference single layer passive film with $L = 1$, $D = 1$, and $S = 1$.

SINGLE-LAYER REACTIVE FILM

We focus on the case where $C_{in} = 0$, which corresponds to a zero partial pressure of the solute inside the package without solute accumulation, that is, with instantaneous removal of the permeated solute from the film–product interface. This is a reasonable assumption for packaged products containing ingredients that are highly sensitive to oxidation, such as vitamins C and E. Then, through the application of Fick's first law, the effective flux [$J_0(t)$] across the downstream boundary $x = 0$ of the reactive film into the packaged product is found as a function of the narrow reaction wavefront position [$L_d(t) = (L \ldots 0)$], as in ref. 4:

$$-J_0(t) \equiv D\left.\frac{dC(x,t)}{dx}\right|_{x=0}$$

$$= \frac{2C_{\text{out}}\sqrt{k_0 D}\,\exp(L_d\sqrt{k_0/D})}{[1+\exp(2L_d\sqrt{k_0/D})][1+(L-L_d)\sqrt{k_0/D}]-2}$$

$$= \frac{DC_{\text{out}}}{L}\frac{2\phi_0 e^{\phi}}{(1+e^{2\phi})(1+\phi_0-\phi)-2} \quad (13)$$

where ϕ is the transient Thiele modulus in the SG model sense, defined as

$$\phi \equiv \phi_{\text{SG}}(t) = L_d(t)\sqrt{\frac{k_0}{D}} \quad (14)$$

The derivative property, called the TR_{eff} or *permeance*, is J_0 normalized to the external solute pressure difference ($\Delta p = p_{\text{out}} - p_{\text{in}}$):

$$TR_{\text{eff}} = -\frac{J_0}{\Delta p} \quad (15)$$

J_0 is negative by definition because its direction is opposite to the imposed external pressure gradient, except in the special case of the reactive barrier with $C_{\text{in}} > C_{\text{in.crit}}$ (where $C_{\text{in.crit}}$ is the critical initial solute concentration at the inner membrane boundary), which results in a transient positive solute flux into the film from both boundaries: this is addressed in part II of this series. The wavefront position (L_d) refers to the location of the narrow reaction zone that is described by a delta-function jump in scavenger concentration (R). The propagating reaction wavefront is assumed to completely consume the scavenger in its wake [$R(x > L_d) = 0$], whereas ahead of the front, the reaction of the scavenger with the permeating solute does not deplete the scavenger [$R(x < L_d) = R_0$], as shown in Figure 2. That approach allowed us to split the homogeneously reactive film into reactive and passive sublayers to be treated separately. The time-dependent variable ϕ is the transient Thiele modulus for the yet unreacted sublayer of the reacting membrane with the variable thickness $L_d(t)$ but the fixed $k_0 = \mu K R_0$ within it. The time to reach L_d ($L_d = L$ at $t = 0$) was found as

$$t = \frac{\mu R_0}{C_{\text{out}}}\left[\frac{(L-L_d)^2}{2D} - \frac{L-L_d}{\sqrt{k_0 D}} + \frac{1}{k_0}\ln\left(\frac{1+\exp(2L\sqrt{k_0/D})}{1+\exp(2L_d\sqrt{k_0/D})}\right)\right]$$

$$= \frac{\mu R_0}{C_{\text{out}}}\frac{L^2}{D}\left[\frac{(1-\xi)^2}{2} - \frac{1-\xi}{\phi_0} + \frac{1}{\phi_0^2}\ln\left(\frac{1+e^{2\phi_0}}{1+e^{2\phi_0\xi}}\right)\right] \quad (16)$$

where $\xi = L_d(t)/L$ is the dimensionless wavefront position coordinate. Then, the SG model scavenger exhaustion time [t_E°], which approximates the time to reach the end of the scavenger reactive capacity, that is, $L_d(t_E^\circ) = 0$, is found from eq. (16) as

$$t_E^\circ = \frac{\mu R_0}{k_0 C_{\text{out}}}\left[\frac{\phi_0^2}{2} + \ln(\cosh(\phi))\right] \quad (17)$$

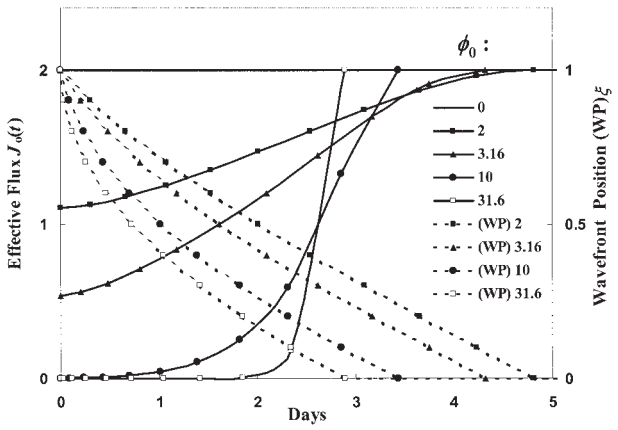

Figure 4 Transient permeance of the reactive monolayer and the reaction wavefront position dynamics: $L = 1$, $D = 1$, $S = 1$, and $\mu R_0 = 1$.

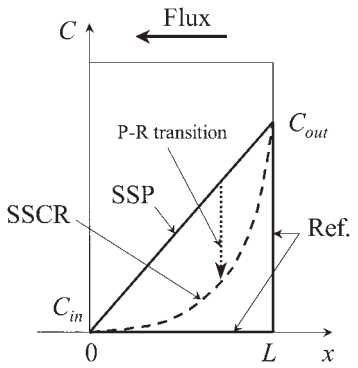

Figure 5 Three types of initial conditions for the solute in the reactive membrane: Ref. = reference condition of the solute free membrane.

Figure 4 demonstrates J_0 and wavefront position dependence on time for different values of ϕ_0. The scavenger exhaustion time estimate t_E° refers to the steady-state initial condition [eq. (7)] for the passive membrane (SSP) or more precisely to the initial conditions of the steady-state permeation through the catalytic reactive membrane (SSCR), as shown in Figure 5. The difference between the SSP and SSCR concentration profiles and the corresponding passive-to-reactive film transition (PRT) were originally discussed in refs. 4 and 6. PRT refers to the solute dynamics in the reactive membrane upon scavenger activation by an external field. In NCR membranes, PRT can be separated from the scavenger consumption dynamics if the

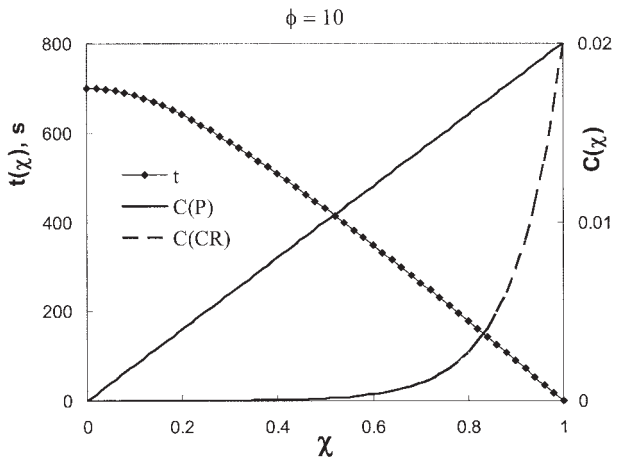

Figure 6 SSP ($\phi = 0$) and SSCR ($\phi_C = 10$) solute concentration profiles in passive and reactive membranes (right scale) and local times to PRT completion (left scale).

reactive capacity (μR_0) of the membrane material is sufficiently large. The effect of PRT on the ingress dynamics was negligible for small values of $\phi_0 \leq 2$. For intermediate ϕ_0 values of interest, $2 < \phi_0 < 100$, and for the SSP initial conditions [eq. (7)], PRT results in an additional ingress and a partial reduction of the scavenger reactive capacity that are not present when the SSCR solute concentration profile is used instead of SSP as the initial condition. For the practically important films with a large μR_0, the relative effect of the PRT on the lag time is diminished due to the fact that the scavenger capacity reduction during the transition is a function of ϕ_0 and the boundary conditions C_{in} and C_{out} only. If the relative reactive capacity of the film material $\Psi = \mu R_0/C_{out} \gg 1$ and $\phi_0 \gg 1$, PRT is rapid compared to the solute diffusion in the membrane, and the latter can be neglected. One can estimate the passive-to-reactive film transition time (t^*) by solving the kinetic equation for solute consumption by the scavenger in the absence of diffusion and defining t^* as the time to undergo transition from a SSP to a SSCR solute concentration profile. It was shown[10] that t^* in CR membranes will also depend on the dimensionless x coordinate $\chi = x/L$:

$$t^*(\chi) = -\frac{1}{k}\ln\left(\frac{C_{CR}(\chi)}{C_P(\chi)}\right) \tag{18}$$

Figure 6 demonstrates the heterogeneity of PRT across the CR layer thickness. For $C_{in} = 0$, the longest transition time occurred at the downstream boundary $x = 0$:

$$t_0^* \equiv t^*(0) = -\frac{1}{k}\ln[\phi_C \mathrm{csch}(\phi_C)] \tag{19}$$

where ϕ_C is the constant Thiele modulus of the CR membrane. Because $\phi_C \gg 1$ was assumed, eq. (19) can be further simplified to yield the overall PRT duration:

$$t_0^* \approx -\frac{1}{k}\ln\left(\frac{2\phi_C}{e^{\phi_C}}\right) = \frac{\phi_C - \ln 2\phi_C}{k} \tag{20}$$

In the vicinity of the downstream boundary $\chi = 0$, the solute concentration will initially evolve as $C(\chi,t) = C_P(\chi)\exp(-kt)$. By the use of this expression and Fick's first law to find $J_0(t)$, the solute ingress $[I(t_0^*)]$ during PRT through the unit barrier area into the downstream volume is found by substituting eq. (19) for t_0^* as

$$I(t_0^*) = -\int_0^{t_0^*} J_0(t)\,dt = D\int_0^{t_0^*}\left(\left.\frac{dC}{dx}\right|_{x=0}\right)dt$$

$$= C_{out}L\,\frac{1 - \phi_C\mathrm{csch}(\phi_C)}{\phi_C^2} \tag{21}$$

Comparison of the overall PRT duration $[t_0^*]$ and the corresponding $I(t_0^*)$ during PRT is shown in Figure 7 as a function of ϕ_C. Equation (21) fails to predict the PRT ingress for $\phi_C < 2$ because solute diffusion during PRT cannot be neglected in the case of slow reaction. For $\phi_C < 2$, the actual ingress will converge to that through the passive film in the limit of $\phi_C \to 0$, as shown in Figure 7. We concluded that in both CR and NCR membranes with a large scavenging capacity where initially $\phi \approx \phi_0 = \phi_C$, the duration of PRT would be short for fast reactions and that the additional ingress during the transition would be negligible. On the other hand, slow reactions result in a negligible solute concentration change throughout the membrane during the transition; therefore, the differ-

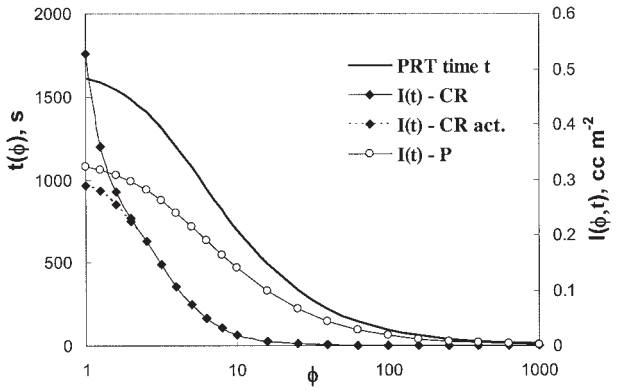

Figure 7 Overall PRT duration as a function of ϕ of the CR membrane (left scale) and the solute ingress during that time [$I(t) - CR$] as predicted by eq. (21) (right scale). The actual ingress for $\phi < 2$ [$I(t) - CR$ act.] and the corresponding ingress through the passive membrane [$I(t) - P$] during the same PRT times are shown as a reference.

ence in the effective flux before and after the transition will be small even if the transition itself takes longer time. For the purposes of this study, the effect of PRT on the transient ingress was not considered, and the SSP initial conditions [eq. (7)] were presumed to be equivalent to the SSCR conditions implied by the original SG model.

t_E° is different from t_L defined for the initially solute-free passive and reactive films (the Ref. line in Fig. 5) as the time delay before establishing asymptotic steady-state flux across the downstream boundary of the film. As previously noted, there is no the steady-state lag time t_L^{SS} shown for the passive film in Figure 4 because the choice of the SSP initial condition [eq. (7)] effectively reduced the time to reach the steady state (t_L^{SS}) to zero. Hence, for the passive film: $t_L^{SSP} \equiv t_L^{SS}(\phi_0 = 0) = 0$.

As noted, the positive permeant ingress [$I(t^*)$] into the package through the unit area of a uniform film during any time interval [0 … t^*] is expressed as

$$I(t^*) = -\int_0^{t^*} J_0(t)\, dt \tag{22}$$

for $-J_0(t) \geq 0$, which is always the case when $C_{\text{in}} = 0$ is maintained. According to the SG model, we can split the ingress in eq. (22) into the ingress through the reactive film [$I_R(t)$] when $t^* \leq t_E^\circ$ and the ingress through the passive film [$I_P(t)$] when $t^* > t_E^\circ$. When the scavenger capacity is exhausted (approximately after t_E°), the steady-state flux (J_x) across any plane x = constant in a homogeneous single layer passive membrane is

$$-J_x = -J^P = TR_{eff}\,\Delta p = \frac{DS\Delta p}{L} \tag{23}$$

The ingress through the passive barrier is then found with eq. (23) as

$$I_P(t_2 - t_1) = -\int_{t_1}^{t_2} J_x\, dt = \frac{DS\Delta p}{L}(t_2 - t_1) = \frac{D}{L}(C_{\text{out}} - C_{\text{in}})(t_2 - t_1) \tag{24}$$

Substituting eqs. (13) and (16) into eq. (22) and replacing integration by t with integration by ξ with the corresponding integration limit change, after routine rearrangements, I_R during the scavenger exhaustion time ($t \leq t_E^\circ$) is

$$I_R(\xi^*) = 2\mu R_0 L\left(\frac{1}{\phi_0}\arctan(e^{\phi_0\xi})\Big|_{\xi^*}^{1} - \int_{\xi^*}^{1}\frac{2e^{\phi_0\xi}}{(1 + e^{2\phi_0\xi})^2[1 + \phi_0(1 - \xi)]}\,d\xi\right) \tag{25}$$

The remaining negative integral in eq. (25) cannot be taken analytically; however, we can estimate its upper bound so that the upper bound estimate of $I_R(t)$ can be obtained for practical purposes. For ξ = [1 … 0], the square bracketed expression in the integral denominator of eq. (25) is bound by

$$1 \leq [1 + \phi_0(1 - \xi)] \leq 1 + \phi_0 \tag{26}$$

When it is replaced by the upper bound

$$[1 + \phi_0(1 - \xi)] \approx 1 + \phi_0 \tag{27}$$

the negative integral in eq. (25) becomes analytical and the upper estimate of the ingress [I_R^+] as a function of time is

$$I_R^+(\xi^*) = \frac{2\mu R_0 L}{1 + \phi_0}\left(\arctan(e^{\phi_0}) - \arctan(e^{\phi_0\xi^*}) - \frac{\text{sech}(\phi_0)}{2\phi_0} + \frac{\text{sech}(\phi_0\xi^*)}{2\phi_0}\right) \tag{28}$$

For the upper estimate of the ingress during the scavenger exhaustion time (at $t = t_E^\circ$; i.e., $\xi^* = 0$) we obtain

$$I_R^+(t_E^\circ) \equiv I_R^+(\xi^* = 0) = \frac{2\mu R_0 L}{1 + \phi_0}\left(\arctan(e^{\phi_0}) - \frac{\pi}{4} - \frac{\text{sech}\phi_0}{2\phi_0} + \frac{1}{2\phi_0}\right) \tag{29}$$

For large ϕ_0 ($\gg$1), the estimate of the ingress during t_E° asymptotically converges to

$$I_R^+(t_E^\circ)\big|_{\phi_0\to\infty} = \frac{\mu R_0 \pi L}{2(1 + \phi_0)} \tag{30}$$

Note that I_R^+ in eqs. (29) and (30) calculated during the exhaustion time does not depend on the boundary conditions when the case of fixed $p_{\text{in}} = 0$ and $p_{\text{out}} > 0$ is considered: t_E° depends on them instead. Figure 8 shows how the normalized ingress estimate depends on ϕ_0; however, keep in mind that the scavenger exhaustion time (t_E; approximated by its SG model estimate t_E°) also depends on ϕ_0, as shown in Figure 4. Hence, the ingress through the reactive film for different values of ϕ_0 in Figure 8 corresponds to different (approximate) scavenger exhaustion times in this film, as shown in the same figure. The ingress predictions for $\phi_0 < 2$ (shown as a dotted line) should be disregarded because such reactive membranes provide negligible barrier improvement compared to passive ones, as discussed earlier. The reason for the ingress underprediction by the SG model at these conditions is the wavefront approximation error in the transient flux introduced by the original SG model[3] and shown

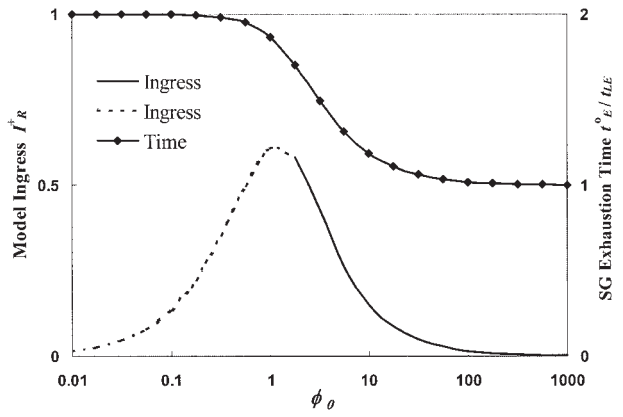

Figure 8 Dependence of the upper ingress estimate during the SG model t_E° on ϕ_0.

in Figure 9. This demonstrates that the initial flux predicted by the SG model coincides with the flux through the CR membrane (as expected) but only for $\phi_0 > 2$. On the other hand, the final SG model flux is proportional to $\phi_0/(1 + \phi_0)$, as follows from eq. (13), instead of being equal to the purely passive flux (normalized to 1 in Fig. 9). The deviation from the passive flux in this case is negative and proportional to $1/(1 + \phi_0)$. That stems from the fact that no well-defined reaction wavefront is present in the reactive layer when ϕ_0 is smaller than 2. In other words, a slow homogeneous reaction consumes the scavenger throughout the membrane thickness rather than in a localized moving reaction zone. The actual scavenger exhaustion time would have to go to infinity as $\phi_0 \to 0$; however, the wavefront approximation in the original SG model effectively limits the exhaustion time estimate at $2t_{LR}^{SS}$ (defined later), as shown in Figure 8, which leads to the overprediction of ingress. Figure 10

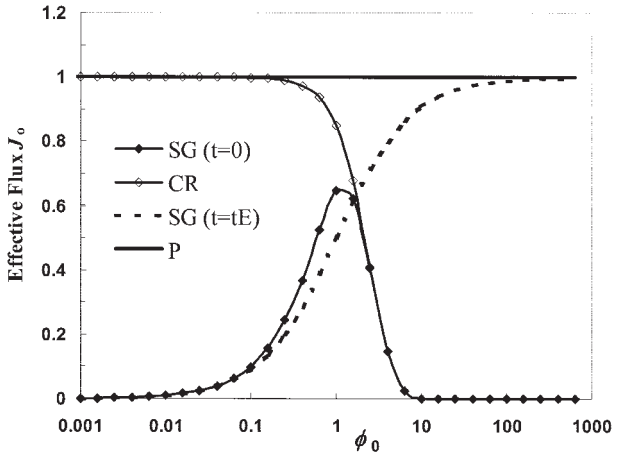

Figure 9 Comparison of the initial ($t = 0$) and final ($t = t_E$) J_0 values through a reactive monolayer as predicted by the SG model (SG) with CR monolayer at $t = 0$ (CR) and passive monolayer at $t = t_E$ (P).

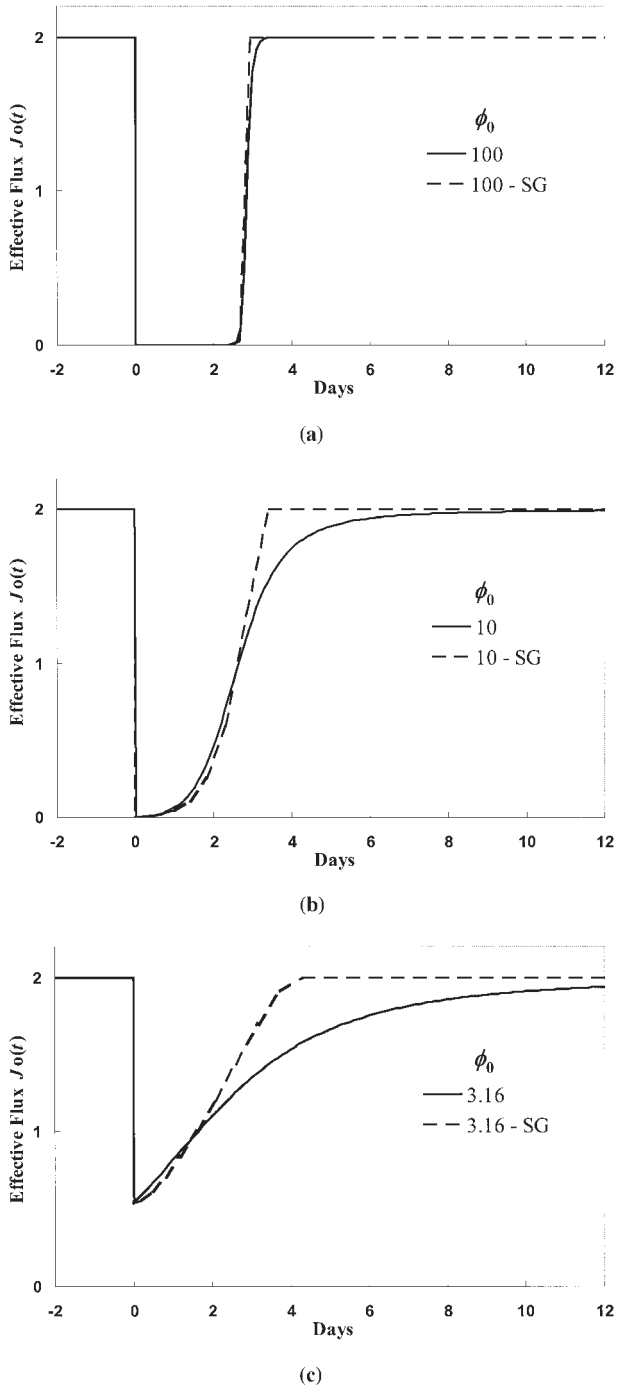

Figure 10 Comparison of transient flux dynamics obtained by numerical simulations with the SG model predictions: ϕ_0 = (a) 100, (b) 10, and (c) 3.16.

demonstrates that the transient flux dynamics is well predicted by the SG model for $\phi_0 > 2$ when compared to numerical simulation results, which thus proves the validity of the model approximations. The flux underprediction of the SG model is more than compensated by the exhaustion time cutoff at $2t_{LR}^{SS}$, which results in an overall ingress overprediction during times longer than and comparable to t_E°. The SG model is extended

to the ingress dynamics through the RP structures in part II of this series. Here, we observe from Figure 10 that higher reaction rates at a fixed reactive capacity of the scavenger can dramatically reduce the solute ingress during the scavenger exhaustion time at the price of shortening the exhaustion time itself.

The scavenger exhaustion time for $k_0 \to \infty$, first obtained by Yang et al.[7] with the impermeable reaction–diffusion wavefront approximation, was formally derived by Siegel and Cussler[8] with a modified method of Frisch[11] for calculating lag times. That time is hereafter called the YNC lag time (t_{LR}^{SS}) or the steady-state lag time due to a noncatalytic scavenging reaction. It is easily obtained from the general results eqs. (16) and (17) as

$$t_{LR}^{SS} = \frac{\mu R_0}{C_{\text{out}}} \frac{L^2}{2D} = \frac{\Psi \phi_0^2}{2k_0} \tag{31}$$

where the dimensionless parameter Ψ is called the relative scavenging capacity of the film material and is defined as

$$\Psi = \frac{\mu R_0}{S p_{\text{out}}} \tag{32}$$

Ψ is a critical parameter of the NCR barrier that relates the absolute scavenging capacity of the polymeric material to the environmental sources of the solute. Although the reaction rate k controls the dynamics of the solute breakthrough across the barrier, Ψ is responsible for the asymptotic behavior, that is, the lag time. Together, these two parameters control the reactive barrier performance, provided the boundary solute concentrations are fixed. Although such a setup is convenient and often used for barrier performance characterization, solute permeation into and out of actual packages with limited volume obviously changes the reactive film environment. Analysis of such complex coupled systems is beyond the scope of this work, although later we present the basic elements of bidirectional solute flow patterns into the reactive membrane, which can be expanded to include variable boundary conditions.

Note that the YNC lag time (t_{LR}^{SS}) is defined for the steady-state initial conditions [eq. (7)] and represents solute permeation across the initially passive membrane. As shown in ref. 4, the t_{LR}^{SS} value in eq. (31) is reduced to zero as $\phi_0 \to 0$ by means of a reduction in the film thickness ($L \to 0$), which provides a transition from eq. (17) for $\phi_0 > 2$ to the asymptotic behavior of t_L^{SS} for the respective passive membrane. If $\phi_0 \to 0$ by means of a reduction in the reaction rate ($k \to 0$) in a film of fixed thickness, t_{LR}^{SS} is conserved. Yang et al. did not distinguish between the scavenger exhaustion time and the lag time because limitations of the YNC model did not allow solute permeation through the reaction wavefront. Therefore, the YNC model predicts the same times for the scavenger exhaustion and the delay before the steady-state permeation was reached, that is, the time when the wavefront traveled through the entire thickness of the reactive layer. This delay is an asymptotic measure of the ingress dynamics at infinite time and whether it is called the reference or steady-state lag time depends on the initial conditions for the solute inside the film. The t_L concept is formally introduced later. The disadvantage of the impermeable wavefront approach is that it always underpredicts the ingress at finite times and, thus, does not always provide a proper perspective for a practitioner analyzing solute breakthrough curves. The SG model on the other hand provides the upper estimate of the ingress for $t \geq t_E^{\circ}$ and, by that, guarantees the actual barrier performance to be equal or better than predicted.

The reference lag time t_L for a homogeneous passive barrier ($\phi_0 = 0$) with uniform L, first introduced by Daynes[12] for the diffusion-caused delay in establishing an asymptotically steady-state flux across an initially solute free film when the solute is suddenly introduced on one side of the membrane, is

$$t_L = \frac{L^2}{6D} \tag{33}$$

There are several well established methods to derive eq. (33), such as the Laplace transform or the method of separation of variables with infinite series expansion summarized in ref. 13. t_L is shown in Figure 3 for the solute ingress dynamics through the passive film at the reference conditions. With t_L in eq. (33) as a reference, t_{LR}^{SS} in eq. (31) can be expressed as

$$t_{LR}^{SS} = 3\Psi t_L \tag{34}$$

Siegel and Cussler[8] rigorously proved that the reference NCR lag time (t_{LR}) has the form

$$t_{LR} = t_L + t_{LR}^{SS} = t_L(1 + 3\Psi) \tag{35}$$

For the inhomogeneous initial scavenger distribution across the membrane thickness $R_0(x) \neq const$ and $C_{in} = 0$, their expression for the steady-state NCR lag time is converted to the coordinate system centered at the downstream membrane boundary as

$$t_{LR}^{SS} = \frac{1}{DC_{out}} \int_0^L \mu R_0(x)(L - x)dx \tag{36}$$

with result (31) being a special case of (36). The additivity of reference passive and steady-state NCR lag

times expressed by (35) is easily confirmed by numerical simulations if one were to compare numerical reference lag time difference ($t_{LR} - t_L$) with the analytical t_{LR}^{SS} value obtained from eq. (31). Numerical t_{LR}^{SS} values are distorted by the PRT mentioned earlier if the SSP initial conditions [eq. (7)] are used, and that results in a slightly reduced numerical t_{LR}^{SS} compared to the analytical value. This fact makes the SG model even more valuable compared to the YNC model based on the impermeable wavefront assumption. Because the SSP initial conditions correspond to practical applications of active packaging, the actual barrier performance of a NCR membrane will be reduced due to PRT effects. The YNC model is unable to capture these effects, and even without taking them into account, it provides a lower (zero) estimate of the transient ingress during finite times. Therefore, the SG model becomes critically important for material selection and reactive barrier design by providing an accurate upper estimate of the transient ingress during any timeframe of interest.

Equation (34) is an important result and was shown in ref. 4 to hold for $C_{in} = 0$, $\phi_0 > 1.5$ and even smaller ϕ_0 values if the film is not very thin (meaning that L is much larger than the characteristic size of the scavenging species). For smaller ϕ_0 values obtained by L reduction, the accelerated sorption of environmental oxygen due to a scavenging reaction may result in a gradual loss of the reactive barrier function.[4] If ϕ_0 is reduced due to a slower scavenging reaction rate k in a film with a fixed thickness, eq. (31) holds for any $\phi_0 > 0$, provided $C_{in} = 0$. Thus, the relative reactive capacity (Ψ) of the NCR membrane, rather than the scavenging reaction rate, determines the ultimate barrier improvement resulting from the use of noncatalytic solute scavengers.

CONCLUSIONS

In part I of this series, we summarized the analysis methodology for scavenger consumption dynamics and solute ingress through homogeneous reactive membranes incorporating a noncatalytic solute scavenger. This methodology is based on the SG model of transient permeation that we developed[2–4] based on the semipermeable reaction wavefront approach. The effects of initial conditions and the passive-to-reactive transition in the membrane after the scavenger activation on the transient ingress were clarified. Part I demonstrates the advantages and importance of the SG model for practical applications and optimized design of reactive barriers compared to the existing models. The solutions [eqs. (13), (16), (17), (28), and (29)] form the core of the SG model for transient permeation and solute ingress through homogeneously reactive single layer films. They will serve as a basis for the analysis of multilayer structures with a NCR layer with the SSP or, more accurately, SSCR initial conditions.

Part II of the series establishes a framework for the transient ingress analysis through the two-layer RP and passive–reactive films. In part III, we analyze specific cases of two-layer RP barriers, introduce generalized solutions for multilayer films, and provide a practical guide to the optimized design of RP barrier structures.

NOMENCLATURE

A	area of the barrier (m^2)
C	solute concentration in the membrane matrix material [mol/m^3 or cm^3 (STP)/m^3]
[C]	solute concentration outside the membrane [mol/m^3 or cm^3 (STP)/m^3]
D	solute diffusivity in the polymer matrix (m^2/s)
$I(t)$	solute ingress through a unit area of the package during the time interval [0…t] [cm^3 (STP)/m^2]
I_P	solute ingress through a unit area of the passive barrier [cm^3 (STP)/m^2]
I_R	solute ingress through a unit area of the reactive barrier [cm^3 (STP)/m^2]
I_R^+	Solovyov–Goldman model estimate of solute ingress through a unit area of the reactive barrier [cm^3 (STP)/m^2]
J_0	effective solute flux across a downstream boundary $x = 0$ of the barrier film [cm^3 (STP) m^{-2} s^{-1}]
J^P	solute flux through a homogeneous passive barrier [cm^3 (STP) m^{-2} s^{-1}]
J_x	solute flux across the membrane plane x = constant [cm^3 (STP) m^{-2} s^{-1}]
$h(t)$	Heaviside step function, $h(t) = \{0, t < 0; 1, t \geq 0\}$
H	solute partition coefficient between adjacent carrier media
Ha	Hatta number (Thiele modulus) for a homogeneous reactive membrane
k	pseudo-first-order reaction rate of solute consumption in the reactive layer ($= \mu KR$; s^{-1})
K	reaction rate constant for solute consumption by the scavenger (m^3 mol^{-1} s^{-1})
k_0	the initial pseudo-first-order reaction rate of the solute consumption in the fully activated reactive layer ($= \mu KR_0$; s^{-1})
K_A	reaction rate constant for the fully activated scavenger at 100% capacity (m^3 mol^{-1} s^{-1})
L	membrane layer thickness (m)
L_d	position of reaction wavefront propagating downstream across the reactive layer thickness (m)
p	partial solute pressure (Pa)
P	permeability coefficient of a particular solute in matrix material [cm^3 (STP) m m^{-2} s^{-1} Pa^{-1}]

p_{in} partial solute pressure inside the package (Pa)
p_{out} partial solute pressure outside the package (Pa)
R concentration of the scavenger in the film material (mol/m^3)
R_0 initial concentration of the scavenger in the film material (mol/m^3)
S solubility coefficient of a particular solute in the polymer matrix [cm^3 (STP) m^{-3} Pa^{-1}]
t time (s)
T temperature (K)
t_E° steady-state Solovyov–Goldman model scavenger exhaustion time for $\phi_0 > 2$ (s)
t_L reference lag time for passive barrier (s)
t_L^+ Solovyov–Goldman model estimate of the steady-state lag time for reactive barrier (s)
t_L^{SS} steady-state lag time for a passive barrier (s)
t_{LR} reference lag time for noncatalytic reactive barrier
t_{LR}^{SS} steady-state lag time for a noncatalytic reactive barrier (s)
TR steady-state transmission rate of the solute through membrane [cm^3 (STP) m^{-2} s^{-1} Pa^{-1}]
TR_{eff} effective transmission rate (permeance) measured at the downstream boundary of the membrane [cm^3 (STP) m^{-2} s^{-1} Pa^{-1}]
x coordinate across membrane thickness L (m)

Greek symbols

μ stoichiometric reactive capacity of the scavenger (mol/mol)
ξ dimensionless position of a reaction wavefront within a membrane
ϕ transient Thiele modulus of unreacted sublayer in a noncatalytic reactive membrane
ϕ_0 initial Thiele modulus of a homogeneous reactive membrane at the moment of uniform scavenger activation throughout the membrane thickness
ϕ_C Thiele modulus of homogeneous catalytic reactive membrane
ϕ_R transient Thiele modulus of noncatalytic reactive layer
ϕ_{SG} transient Thiele modulus of noncatalytic reactive layer in the Solovyov–Goldman model sense
χ dimensionless x coordinate across membrane thickness ($= x/L$)
Ψ relative scavenging capacity of the membrane material

References

1. (a) Speer, D. V.; Morgan, C. R.; Roberts, W. P.; VanPutte, A. W.; U.S. Pat. 5,529,833, 1996; (b) Speer, D. V.; Roberts, W. P.; Morgan, C. R.; Ebner, C. L.; U.S. Pat. 5,700,554, 1997; (c) Gauthier, W. J.; Speer, D. V.; U.S. Pat. 5,981,676, 1999; (d) Adur, A. M.; Marano, G. A.; Volpe, R. A.; Mei, H. L.; U.S. Pat. 6,037,022, 2000; (e) Carr, D. G.; Castner, G. C.; DelDuca, G. R.; DeMay, R. H.; Deyo, A. E.; Goulette, S. L.; Hansen, D. P.; Luthra, V. K.; Norby, A. J.; Sloan, R. A.; Thompson, J. S.; U.S. Pat. 6,054,153, 2000; (f) Colombo, E. A.; U.S. Pat. 6,112,890, 2000; (g) Carr, D. G.; Castner, G. C.; DelDuca, G. R.; DeMay, R. H.; Deyo, A. E.; Goulette, S. L.; Hansen, D. P.; Luthra, V. K.; Norby, A. J.; Sloan, R. A.; Thompson, J. F.; U.S. Pat. 6,132,781, 2000; (h) Gauthier, W. J.; Speer, D. V.; U.S. Pat. 6,143,197, 2000; (i) Finkelstein H.; Burns, B.; Flores, V.; McKenna, R.; Verdel, A.; U.S. Pat. 6,194,042, 2001; (j) DelDuca, G. R.; Deyo, A. E.; Luthra, V. K.; Wu, V. P.; U.S. Pat. 6,231,905, 2001; (k) Bansleben, D. A.; Opuszko, S.; Speer, D. V.; U.S. Pat. 6,255,248, 2001; (l) Cahill, P. J.; Richardson, J. A.; Rotter, G. E.; Smyser, G. L.; Barski, R. F.; Wass, R. V.; Nyderek, W. M.; U.S. Pat. 6,346,308, 2002; (m) Akkapeddi, M. K.; Kraft, T. J.; Socci, E. P.; U.S. Pat. 6,423,776, 2002; (n) Tsai, M. L.; Akkapeddi, M. K.; U.S. Pat. 6,479,160, 2002; (o) Cahill, P. J.; Rotter, G. E.; Chen. S. Y.; U.S. Pat. 6,558,762,2003.
2. Solovyov, S. E.; Goldman, A. Y. Int J Polym Mater 2005, 54, 71.
3. Solovyov, S. E.; Goldman, A. Y. Int J Polym Mater 2005, 54, 93.
4. Solovyov, S. E.; Goldman, A. Y. Int J Polym Mater 2005, 54, 117.
5. Paul, D. R.; Koros, W. J. J Polym Sci Polym Phys Ed 1976, 14, 675.
6. Solovyov, S. E. J Phys Chem B 2004, 108, 15618.
7. Yang, C.; Nuxoll, E. E.; Cussler, E. L. AIChE J 2001, 47, 295.
8. Siegel, R. A.; Cussler, E. L. J Membr Sci 2004, 229, 33.
9. Siegel, R. A. J Phys Chem 1991, 95, 2556.
10. Solovyov, S. E., unpublished results, 2005.
11. Frisch, H. L. J Phys Chem 1957, 61, 93.
12. Daynes, H. A. Proc R Soc London Ser A 1920, 97, 286.
13. Crank, J. The Mathematics of Diffusion, 2nd ed.; Clarendon: Oxford, 1975.